AD-A057 260 DAVID W TAYLOR NAVAL SHIP RESEARCH AND DEVELOPMENT CE--ETC F/G 20/4
NASTRAN IMPLEMENTATION FOR FREE SURFACE FLOW PROBLEMS.(U)
AUG 78 P R ZARDA, M S MARCUS

UNCLASSIFIED DTNSRDC-78/065 NL

| OF |
AD
A057 260

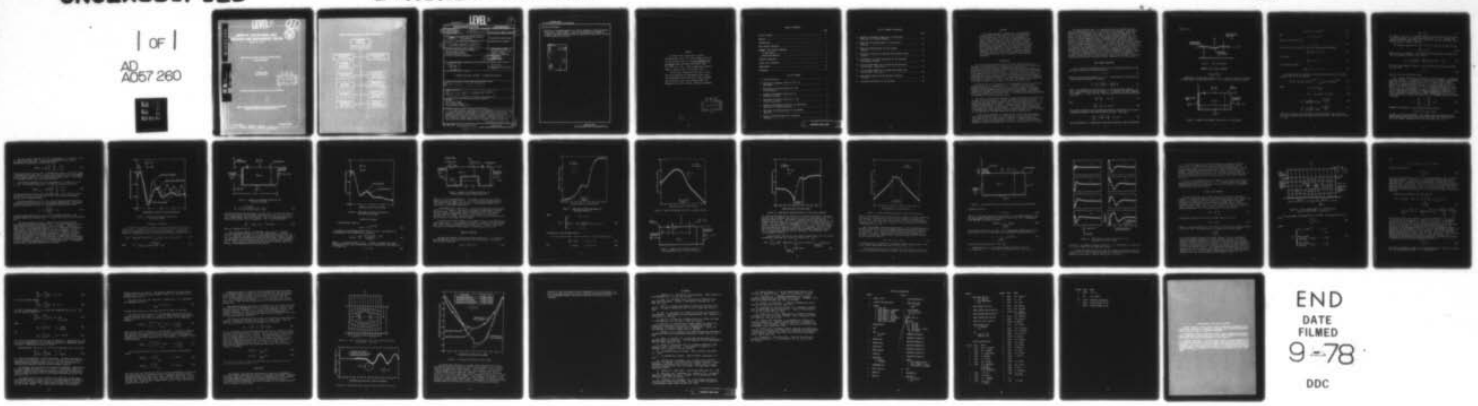

END
DATE
FILMED
9-78
DDC

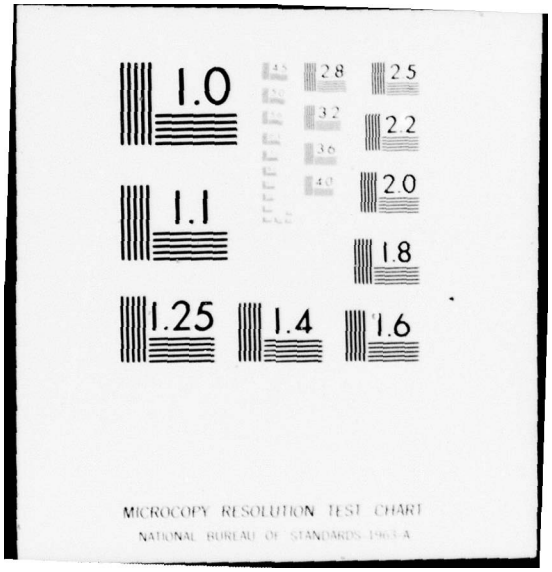
1.0
1.1
1.25
1.4
1.6
2.8
3.2
3.6
4.0
2.5
2.2
2.0
1.8
MICROCOPY RESOLUTION TEST CHART
NATIONAL BUREAU OF STANDARDS-1963-A

DAVID W. TAYLOR NAVAL SHIP
RESEARCH AND DEVELOPMENT CENTER
Bethesda, Md. 20084

NASTRAN IMPLEMENTATION FOR FREE SURFACE FLOW PROBLEMS

by

P. Richard Zarda
Melvyn S. Marcus

COMPUTATION, MATHEMATICS, AND LOGISTICS DEPARTMENT
RESEARCH AND DEVELOPMENT REPORT

August 1978

DTNSRDC-78/065

NASTRAN IMPLEMENTATION FOR

MAJOR DTNSRDC ORGANIZATIONAL COMPONENTS

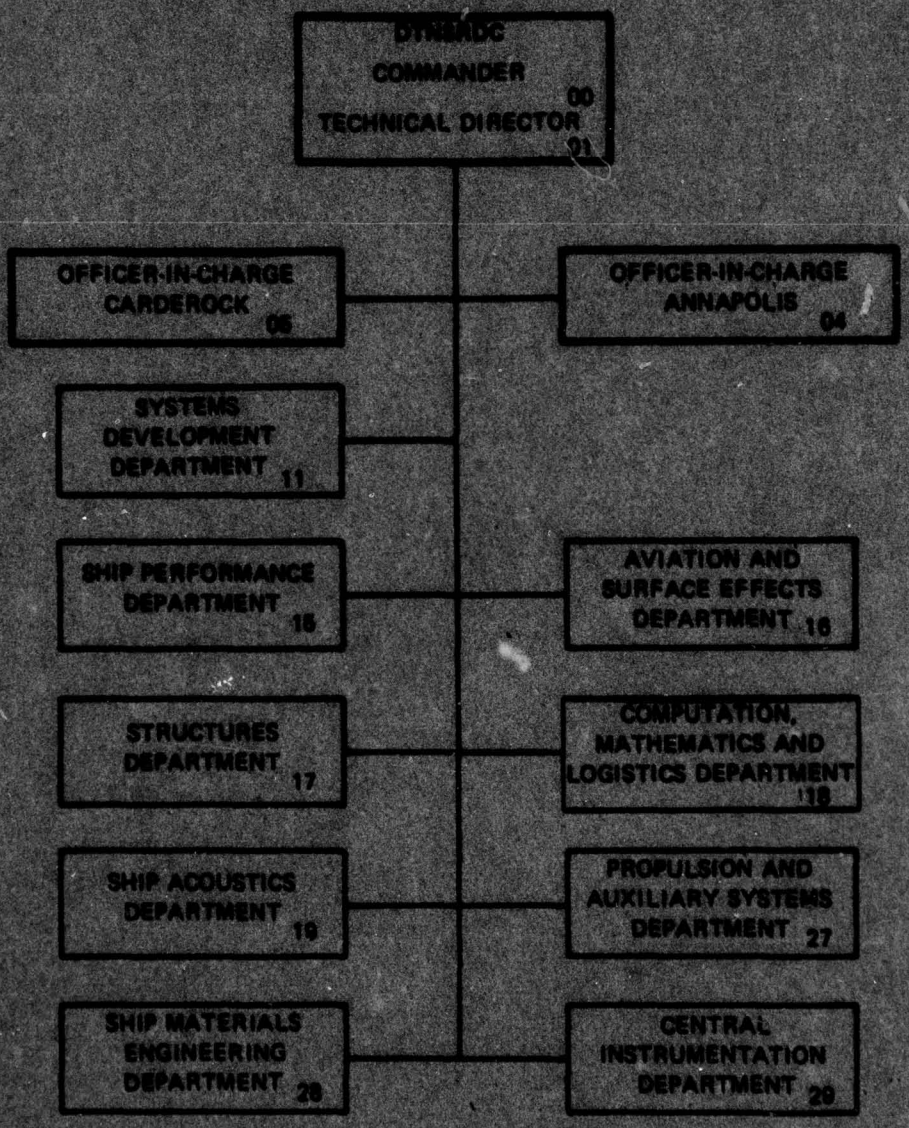

UNCLASSIFIED

LEVEL II

(11)

SECURITY CLASSIFICATION OF THIS PAGE (When Data Entered)

REPORT DOCUMENTATION PAGE

READ INSTRUCTIONS BEFORE COMPLETING FORM

(14) 1. REPORT NUMBER: DTNSRDC-78/065

(9) 2. GOVT ACCESSION NO.

3. RECIPIENT'S CATALOG NUMBER

Research and development rept.

(6) 4. TITLE (and Subtitle): NASTRAN IMPLEMENTATION FOR FREE SURFACE FLOW PROBLEMS.

5. TYPE OF REPORT & PERIOD COVERED

6. PERFORMING ORG. REPORT NUMBER

(10) 7. AUTHOR(s): P. Richard Zarda and Melvyn S. Marcus

8. CONTRACT OR GRANT NUMBER(s)

9. PERFORMING ORGANIZATION NAME AND ADDRESS
David W. Taylor Naval Ship Research and Development Center
Bethesda, Maryland 20084

10. PROGRAM ELEMENT, PROJECT, TASK AREA & WORK UNIT NUMBERS
Program Element: 61152N
Project: Z0140201
Work Unit: 1-1844-109

11. CONTROLLING OFFICE NAME AND ADDRESS

(11) 12. REPORT DATE: August 1978

13. NUMBER OF PAGES: 37

(12) 34 p.

14. MONITORING AGENCY NAME & ADDRESS (if different from Controlling Office)

15. SECURITY CLASS. (of this report): UNCLASSIFIED

15a. DECLASSIFICATION/DOWNGRADING SCHEDULE

16. DISTRIBUTION STATEMENT (of this Report)

APPROVED FOR PUBLIC RELEASE: DISTRIBUTION UNLIMITED.

17. DISTRIBUTION STATEMENT (of the abstract entered in Block 20, if different from Report)

(16) Z0140 2, SR0140 3

18. SUPPLEMENTARY NOTES

(17) Z0140201, SR0140301

19. KEY WORDS (Continue on reverse side if necessary and identify by block number)
NASTRAN
Free Surface Flows
Finite Element Method
Fluid-Structure Interaction

20. ABSTRACT (Continue on reverse side if necessary and identify by block number)

This paper presents a procedure for using NASTRAN to determine the flow field about arbitrarily shaped bodies in the presence of a free surface. The fundamental unknown of the problem is the velocity potential which must satisfy Laplace's equation in the fluid region. Boundary conditions on the free surface may involve second order derivatives in space and time. In cases involving infinite domains either a tractable radiation condition is

(Continued on reverse side)

next page

16

DD FORM 1 JAN 73 1473 EDITION OF 1 NOV 65 IS OBSOLETE
S/N 0102-014-6601

UNCLASSIFIED
SECURITY CLASSIFICATION OF THIS PAGE (When Data Entered)

387682

(Block 20 continued)

applied at a truncated boundary or a series expansion is used and matched to the local finite elements. Solutions are presented for harmonic, transient, and steady state problems and compared to either exact solutions or other numerical solutions.

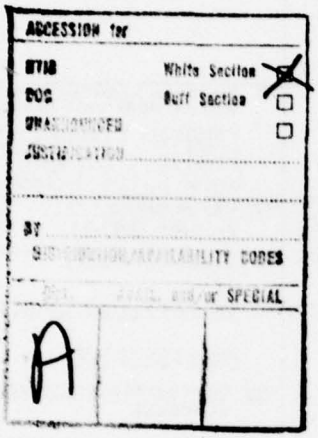

PREFACE

The bulk of this report was originally published under the title "Finite Element Solutions of Free Surface Flows" in the Sixth NASTRAN Users' Colloquium, NASA Conference Publication 2018, Oct. 1977, pp. 27-52. (Held at NASA-Lewis Research Center, Cleveland, Ohio, 4-6 October 1977.)

The work was supported by the David W. Taylor Naval Ship Research and Development Center under the Independent Research Program, Project Z0140201, and by the Naval Sea Systems Command under the Mathematical Sciences Program, Subproject SR0140301.

TABLE OF CONTENTS

	Page
LIST OF FIGURES	v
ABSTRACT	1
INTRODUCTION	1
FREE SURFACE EQUATIONS	2
HARMONIC FREE SURFACE PROBLEMS	3
2-D WAVE MAKER	3
REFRACTION PROBLEMS	9
TRANSIENT PROBLEMS	10
STEADY STATE PROBLEMS	17
CONCLUSIONS	22
REFERENCES	27

LIST OF FIGURES

1 - Free Surface Wave	3
2 - Geometry and Boundary Conditions for 2-D Wave Maker	3
3 - Amplitude of Surface Elevation for the 2-D Wave Maker	7
4 - Geometry and Boundary Conditions for Pulsating Cylinder	8
5 - Amplitude of Surface Elevation for the Pulsating Cylinder	9
6 - Geometry and Boundary Conditions for Refracted Waves Due to a Bottom Obstacle	10
7 - Amplitude of Refracted Waves for the Bottom Obstacle	11
8 - Phase of Refracted Waves for the Bottom Obstacle	12

LIST OF FIGURES (Continued)

	Page
9 - Geometry and Boundary Conditions for Refracted Waves Due to a Surface Obstacle	12
10 - Amplitude of Refracted Waves for the Surface Obstacle	13
11 - Phase of Refracted Waves for the Surface Obstacle	14
12 - Stationary Pressure Distribution Oscillating on Free Surface	15
13 - Development of Surface Elevations for the Pressure Distribution Problem	16
14 - Finite Element Model for Cylinder Moving Below the Free Surface - Coarse Grid	18
15 - Finite Element Model for Cylinder Moving Below the Free Surface - Fine Grid	23
16 - Wave Height Along the Free Surface for Moving Cylinder	23
17 - Pressure Distribution on the Cylinder	24

ABSTRACT

This paper presents a procedure for using NASTRAN to determine the flow field about arbitrarily shaped bodies in the presence of a free surface. The fundamental unknown of the problem is the velocity potential which must satisfy Laplace's equation in the fluid region. Boundary conditions on the free surface may involve second order derivatives in space and time. In cases involving infinite domains either a tractable radiation condition is applied at a truncated boundary or a series expansion is used and matched to the local finite elements. Solutions are presented for harmonic, transient, and steady state problems and compared to either exact solutions or other numerical solutions.

INTRODUCTION

The pressure distribution and flow field about submerged bodies are important in the determination of hydrodynamic variables such as lift and wave resistance and the calculation of boundary-layer characteristics. The investigation of these variables can be realistically modeled by assuming the fluid to be inviscid and incompressible. In this case the equations of motion can be reduced to the solution of Laplace's equation in the fluid region. The linearized free surface condition (small wave amplitude) may involve second derivatives of the velocity potential ϕ in both space and time and considerably complicates the problem. The free surface flows investigated in this paper can be divided into three areas: harmonic, transient, and steady state.

An exhaustive list of literature for forced harmonic motion or diffraction problems may be found in Wehausen (ref. 1). Problems of this type were generally solved by using a distribution of sources or dipoles on the body boundary with an appropriate Green's function for the problem. The boundary condition on the body is used to determine the strength of the source distribution (for example, Hess and Smith, ref. 2). Such solutions are appropriate only for problems of infinite or constant depth.

Bai (refs. 3-6) uses finite elements to model both harmonic and steady state problems of arbitrary geometry. Similar methods which employ variational functionals have been used by Berkhoff (ref. 7) and Chen and Mei (ref. 8). For steady state problems Bai developed a localized finite element method (ref. 6) in which finite elements are used in a localized region around the body and a series expansion is used in the remainder. The finite element representation is matched to the series expansion along the common boundary to form a consistent set of equations for the nodal potentials and series coefficients.

Finite element solutions for transient free surface flows are given by Visser and van der Wilt (ref. 9). Unfortunately, for the transient problem there seems to be no suitable method to construct a completely absorbing boundary in cases involving radiation conditions. For that reason truncated boundaries are taken far enough away so as not to affect the region of interest.

The purpose of this paper is to demonstrate how the structural analysis computer program NASTRAN (refs. 10-11) may be used to implement finite element procedures for modeling the three types of free surface problems described above. The use of NASTRAN is motivated by the wide-ranging capability, convenience of use, and availability of this general purpose computer code. The variety of finite elements available in NASTRAN permits the method presented here for 2-D and axisymmetric problems to be routinely applied to complex 3-D geometries of naval and marine interest. In contrast with specialized programming efforts, NASTRAN implementation of the finite element procedures is enhanced by a variety of pre- and postprocessing programs (ref. 12) which include capabilities for automatic data generation, data checking via interactive graphics, matrix bandwidth and profile reduction via grid point resequencing, and contour plots (in the case of scalar variables such as velocity potential) of computer output. In addition, the NASTRAN capability to model free surface flow problems is currently being exploited to investigate the coupled fluid-structure interaction problem involving fluid flow about an elastic body near or on a free surface.

FREE SURFACE EQUATIONS

For an inviscid, incompressible fluid in an irrotational flow field, the equations of motion and continuity reduce to

$$\nabla^2 \Phi = 0 \tag{1}$$

where Φ is the velocity potential (ref. 13). The pressure p in the fluid can be determined from Bernoulli's equation,

$$-\frac{p}{\rho} = \frac{\partial \Phi}{\partial t} + \frac{1}{2}\left[\left(\frac{\partial \Phi}{\partial x}\right)^2 + \left(\frac{\partial \Phi}{\partial y}\right)^2\right] + gy \tag{2}$$

where ρ is the density of the fluid and g is the gravitational constant. In Fig. 1 the deflection of the free surface η is assumed to be small compared to the depth d. In that case the linearized conditions on the free surface are (ref. 10)

$$\frac{\partial \eta}{\partial t} = \frac{\partial \Phi}{\partial y} \quad \text{on} \quad y=0 \tag{3}$$

and

$$\frac{\partial \Phi}{\partial t} = -\frac{p}{\rho} - g\eta \quad \text{on} \quad y=0 \tag{4}$$

The surface elevation η may be eliminated from Eqs. (3) and (4) at the cost of increasing the order of the time derivatives by one. This gives

$$\frac{\partial^2 \Phi}{\partial t^2} = -\frac{1}{\rho}\frac{\partial p}{\partial t} - g\frac{\partial \Phi}{\partial y} \quad \text{on} \quad y=0 \tag{5}$$

Once the potential Φ is determined, the surface elevation η may be determined

from Eq. (4).

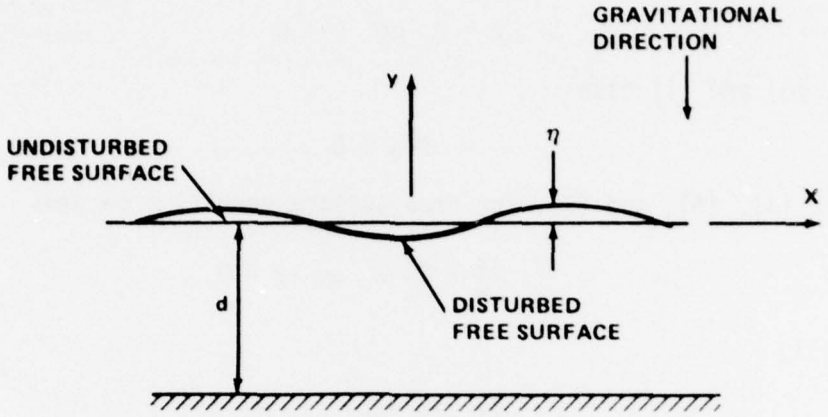

Figure 1. Free Surface Wave

HARMONIC FREE SURFACE PROBLEMS

2-D Wave Maker

Consider the 2-D wave maker shown in Fig. 2. At x=0, a wall is oscillating in simple harmonic motion with velocity V. For the harmonic problems, assume

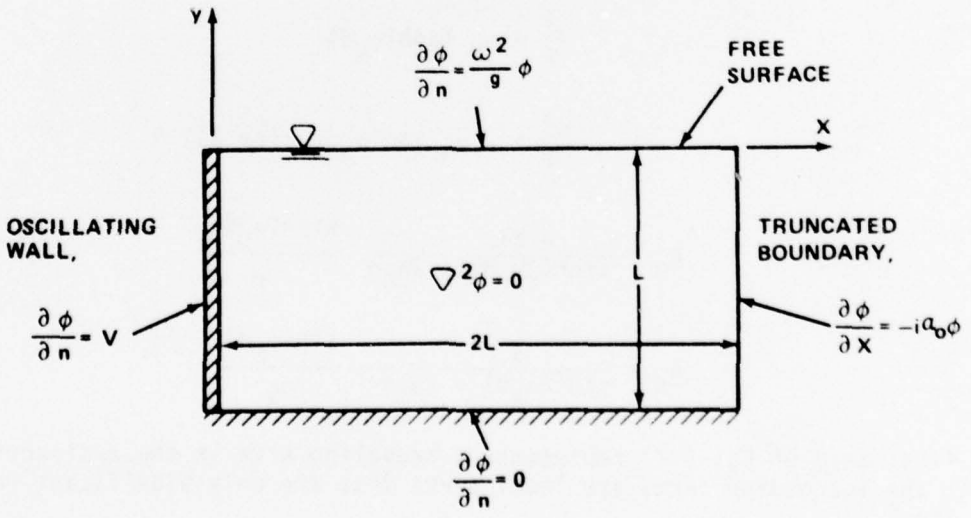

Figure 2. Geometry and Boundary Conditions for 2-D Wave Maker

$$\phi(x,y,t) = \phi(x,y)\, e^{i\omega t} \tag{6}$$

and

$$p = 0 \quad \text{on} \quad y = 0 \tag{7}$$

Then Eqs. (6) and (1) give

$$\nabla^2 \phi = 0 \tag{8}$$

Using Eqs. (5), (6), and (7), the free surface condition becomes

$$\frac{\partial \phi}{\partial y} = \frac{\omega^2}{g} \phi \quad \text{on} \quad y = 0 \tag{9}$$

At the wall,

$$\frac{\partial \phi}{\partial n} = V \quad \text{on} \quad x = 0 \tag{10}$$

and, along the bottom,

$$\frac{\partial \phi}{\partial n} = 0 \quad \text{on} \quad y = -d = -L \tag{11}$$

The solution of this problem can be obtained by separation of variables (see Bai, ref. 3) and is given by

$$\phi(x,y) = A_0 \cosh \alpha_0(y+d) e^{-\alpha_0 ix} + \sum_{N=1}^{\infty} A_N \cos \alpha_N(y+d) e^{-\alpha_N x} \tag{12}$$

where

$$\frac{\omega^2}{g} = \alpha_0 \tanh(\alpha_N d) \tag{13}$$

$$\frac{\omega^2}{g} = -\alpha_N \tan(\alpha_N d) \quad \text{for all } N \tag{14}$$

$$A_0 = \frac{-4i}{\sinh(2\alpha_0 d) + 2\alpha_0 d} \frac{\sinh(\alpha_0 d)}{\alpha_0} \tag{15}$$

$$A_N = \frac{4}{\sin(2\alpha_N d) + 2\alpha_N d} \frac{\sin(\alpha_N d)}{\alpha_N} \tag{16}$$

The first term of Eq. (12) represents a traveling wave in the x-direction, while the succeeding terms are local terms that are only significant for small x. Thus

$$\frac{\partial \phi}{\partial x} = -i\,\alpha_0\,\phi \tag{17}$$

for large x. Eq. (17) is a tractable radiation condition which can be applied at suitable boundary far enough away from the wall. Eq. (8), together with boundary conditions given by Eqs. (9), (10), (11), and (17), constitute a well-posed problem for Laplace's equation.

The boundary conditions Eqs. (9), (10), (11), and (17) all have the form

$$\frac{\partial \phi}{\partial n} + \gamma\phi = \beta \tag{18}$$

where γ and β are constants. The functional form for Laplace's equation with the mixed boundary condition of Eq. (18) is

$$F(\phi) = \frac{1}{2}\iint_A \left\{\left(\frac{\partial \phi}{\partial x}\right)^2 + \left(\frac{\partial \phi}{\partial y}\right)^2\right\} dA + \int_B \left(\frac{1}{2}\gamma\phi^2 - \beta\phi\right) ds \tag{19}$$

where B is the boundary of region A. When variations are taken with respect to ϕ such that

$$\delta F = 0 \tag{20}$$

then Eqs. (8) and (18) are satisfied.

Eqs. (19) and (20) can be approximated with finite elements using NASTRAN structural elements. A procedure for using structural elements to model fluid domains which satisfy the wave equation (or, as a special case, Laplace's equation) is given by Everstine et al (ref. 14), and has been successfully applied using NASTRAN on several problems by Schroeder and Marcus (ref. 15), Marcus (ref. 16), and Everstine (ref. 17). A translational degree of freedom (in this case the x displacement) is chosen to represent the potential ϕ, and all other degrees of freedom at a node are permanently constrained. The linear isoparametric membrane element, QDMEM1 (NASTRAN Level 16), was used. The material matrix $\underline{G}$ and the mass density ρ_e of the QDMEM1 elements are chosen as follows:

$$\underline{G} = \begin{bmatrix} 1 & -1 & 0 \\ -1 & 1 & 0 \\ 0 & 0 & 1 \end{bmatrix}, \quad \rho_e = 0 \tag{21}$$

NASTRAN's Rigid Format 8, with governing equation given by

$$(-\omega^2 \underline{M} + i\,\omega \underline{B} + \underline{K})\,\underline{\phi} = \underline{F}(\omega) \tag{22}$$

is chosen as the analysis method. The stiffness matrix $\underline{K}$ generated by the QDMEM1 elements with material properties given by Eq. (21) is equivalent to the finite element representation of the first term in Eq. (19).

The free surface condition, Eq. (9), corresponds to $\gamma = \omega^2/g$ and $\beta = 0$ in the second term of Eq. (19). A consistent formulation for this term is implemented using NASTRAN by inserting the matrix

$$(M2PP)_{i,j} = \frac{\Delta x}{6g} \begin{bmatrix} 2 & 1 \\ 1 & 2 \end{bmatrix}, \quad \begin{matrix} i=k,\ell \\ j=k,\ell \end{matrix} \tag{23}$$

into the mass matrix $\underline{M}$ in Eq. (22) using DMIG data cards. In Eq. (23), k and ℓ represent the two nodes which lie on the free surface for each of the QDMEM1 surface elements, while Δx is the spacing between nodes k and ℓ. The frequency ω is inserted into Eq. (22) using a FREQ data card.

The radiation condition, Eq. (17), corresponds to $\beta = 0$ and $\gamma = i\,\alpha_0$ in Eq. (19). A consistent formulation is obtained by inserting the matrix

$$(M2PP)_{i,j} = -\,i\,\frac{\alpha_0}{\omega^2}\,\frac{\Delta y}{6} \begin{bmatrix} 2 & 1 \\ 1 & 2 \end{bmatrix}, \quad \begin{matrix} i=k,\ell \\ j=k,\ell \end{matrix} \tag{24}$$

into the mass matrix $\underline{M}$ in Eq. (22) using DMIG cards. In Eq. (24) k, ℓ, and Δy are defined as in Eq. (23) except that in this case the relevant boundary surface is the truncated boundary.

The bottom condition, Eq. (11), is a natural boundary condition which is automatically satisfied within the finite element approximation. The boundary condition at the wall, Eq. (10), is implemented by inserting the vector

$$F_i = V\,\Delta y \begin{bmatrix} 1/2 \\ 1/2 \end{bmatrix}, \quad i=k,\ell \tag{25}$$

into the forcing function $\underline{F}(\omega)$ in Eq. (22) using DAREA data cards. The relevant boundary for the quantities k, ℓ, and Δy in Eq. (25) is the oscillating wall.

The above procedure was used to compute the fluid response for the oscillating wall problem illustrated in Fig. 2. All data is presented in non-dimensionalized form using the length L and the velocity V. Results are shown in Fig. 3 for dimensionless spacing $\Delta x = \Delta y = .0625$ which corresponds to approximately 10 nodes per wave length for the linear elements. In Fig. 3, the amplitude of the surface elevation is plotted. The NASTRAN solutions obtained by both consistent and lumped formulations, as well as the analytic solution, are presented. The lumped formulation is determined by using diagonalized matrices in Eqs. (23) and (24) where diagonal terms are determined by adding together all terms in the corresponding row. The consistent formulation is a significant improvement over the lumped formulation. In subsequent problems only a consistent formulation will be used.

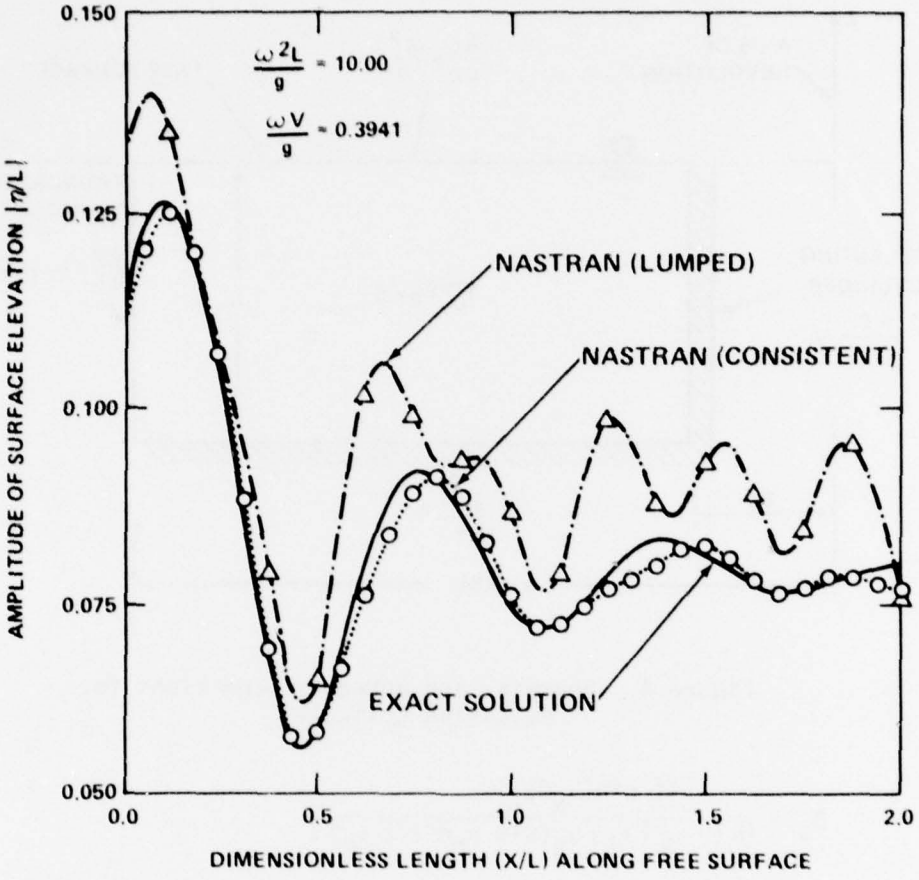

Figure 3. Amplitude of Surface Elevation for the 2-D Wave Maker

Axisymmetric Wave Maker

The geometry and boundary conditions for the axisymmetric wave maker are shown in Fig. 4. Boundary conditions are the same as for the 2-D wave maker except for the additional term in the radiation condition. The radiation condition is determined by investigating the exact solution (see Bai, ref. 3):

$$\phi(r,z) = B_0 H_0(\alpha_0 r) \cosh \alpha_0 (z+d) + \sum_{N=1}^{\infty} B_N H_0(-\alpha_N i r) \cos \alpha_N (z+d) \qquad (26)$$

where $$B_0 = \frac{4 \sinh(\alpha_0 d)}{H_1(\alpha_0 r_0)\, \alpha_0 \{\sinh(\alpha_0 d) + 2\alpha_0 d\}} \qquad (27)$$

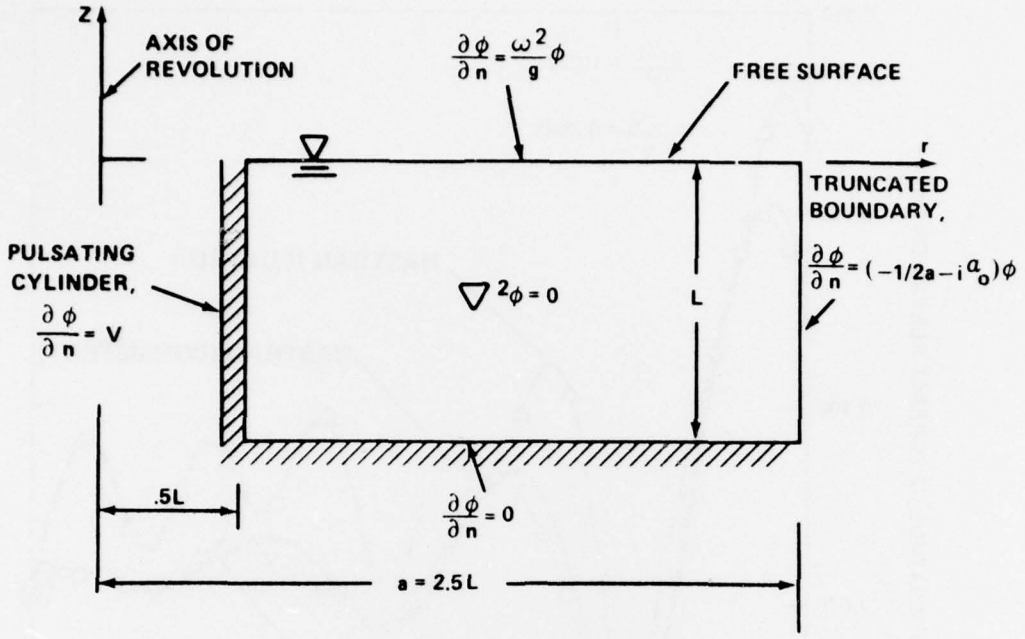

Figure 4. Geometry and Boundary Conditions for Pulsating Cylinder

$$B_N = \frac{4i \sin(\alpha_N d)}{H_1(-\alpha_N i r_0)\alpha_N\{\sin \alpha_N d + 2\alpha_N d\}} \tag{28}$$

and where α_0 and α_N are given by Eqs. (13) and (14), r_0 is the inner radius of the cylinder, and H_0, H_1 are Hankel functions of the second kind of order 0 and 1, respectively. The first term of Eq. (26) is an outgoing wave and the second terms represent local disturbances. Thus it can be shown that

$$\frac{\partial \phi}{\partial r} = -\left\{\frac{1}{2a} + i\alpha_0\right\}\phi \quad \text{for large } r \tag{29}$$

where a is defined in Fig. 4.

This problem was modeled using NASTRAN's Rigid Format 8. CTRAPRG elements were used (Everstine, ref. 17) with dimensionless spacing given by $\Delta x = \Delta y = .0625$ (all variables are non-dimensionalized with respect to V and L). This corresponds to approximately 10 nodes per wave length. Results showing the amplitude of the surface elevation along the free surface are presented in Fig. 5. These results are based on applying consistent boundary conditions, and are in good agreement with the series solution.

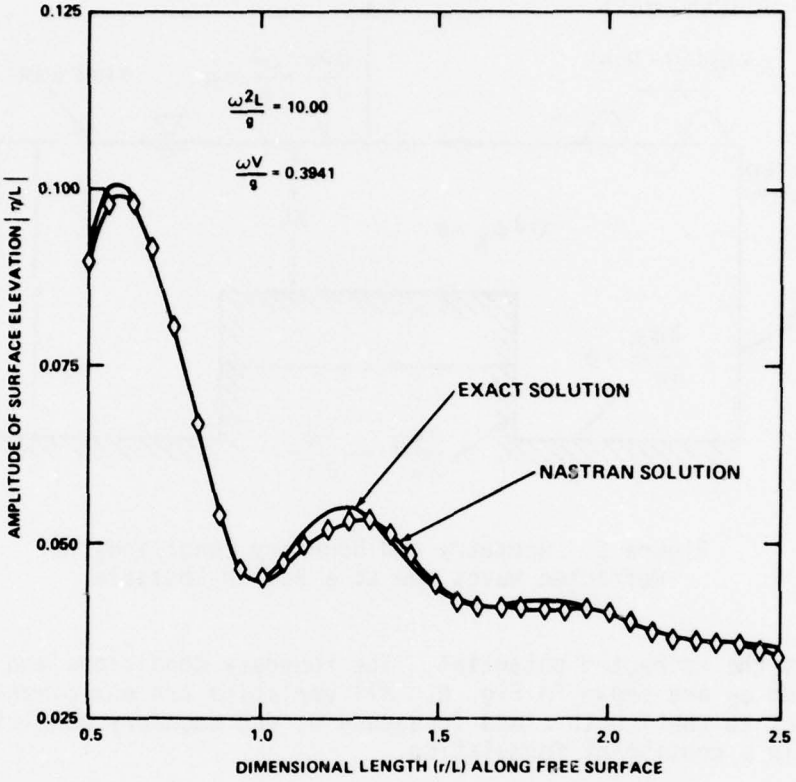

Figure 5. Amplitude of Surface Elevation for the Pulsating Cylinder

Refraction Problems

A surface wave, given by

$$\eta(x,t) = A\, e^{i(\omega t - \alpha_0 x)} \tag{30}$$

is incident upon the bottom obstacle shown in Fig. 6. The potential ϕ_I corresponding to the incident wave is given by

$$\Phi_I(x,y) = \frac{Ag\,i}{\omega} \frac{\cosh \alpha_0 (y+d)}{\cosh(\alpha_0 d)} e^{-i\alpha_0 x} \tag{31}$$

where ω, α_0, g, and d satisfy Eq. (13). In order to determine the total potential ϕ of the fluid corresponding to the incident wave, the potential ϕ is divided into

$$\phi = \phi_I + \phi_R \tag{32}$$

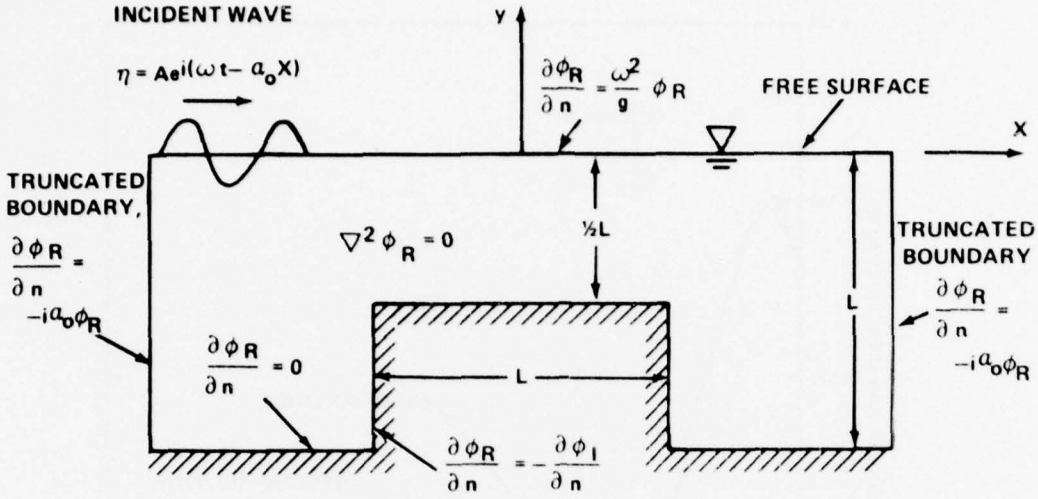

Figure 6. Geometry and Boundary Conditions for Refracted Waves Due to a Bottom Obstacle

where ϕ_R is the refracted potential. The boundary conditions and governing equations on ϕ_R are shown in Fig. 6. All variables are non-dimensionalized with respect to the length L and frequency ω, and boundary conditions are specified in a consistent formulation.

The NASTRAN results shown in Figs. 7 and 8 are presented for dimensionless spacing $\Delta x = .125$ and $\Delta y = .0625$, which corresponds to approximately 41 nodes per wave length. These results compare favorably with the finite element solution recently re-computed by Bai as a correction to his originally published (ref. 5) results. Accuracies within 4% have also been obtained using coarser grids of 10-20 nodes per wave length.

A similar free surface problem is illustrated in Fig. 9. The dimensionless spacing used was $\Delta x = \Delta y = .125$, which corresponds to approximately 42 nodes per wave length. Again, the NASTRAN results shown in Figs. 10 and 11 compare well with the finite element solution recently re-computed by Bai (ref. 5).

TRANSIENT PROBLEMS

Consider the transient free surface problem shown in Fig. 12 illustrating the time dependent pressure distribution on the free surface. The pressure distribution is given by

$$p(x,t) = P(x) \sin \omega t \qquad (33)$$

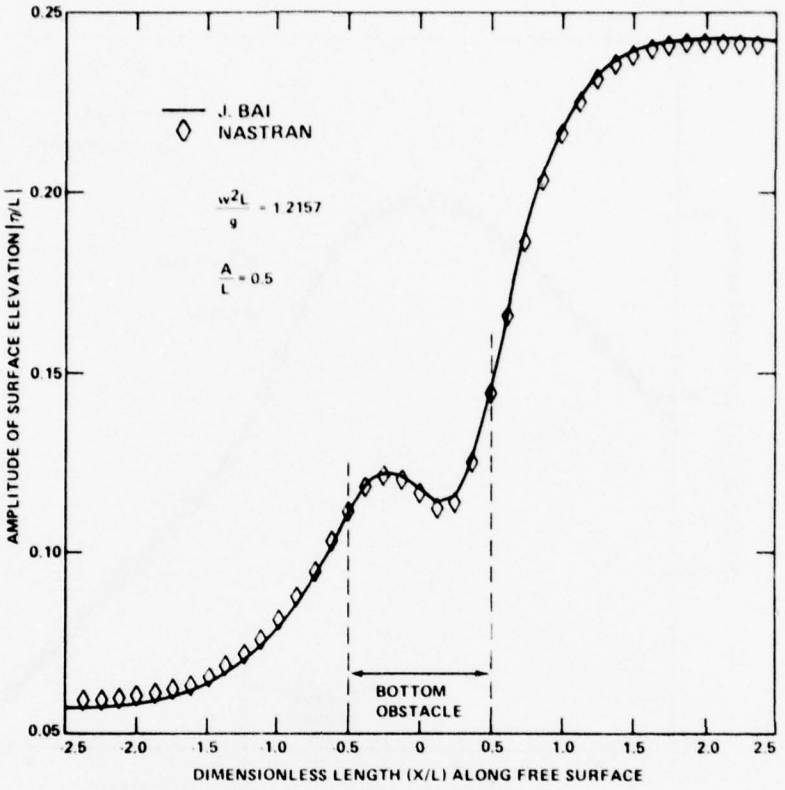

Figure 7. Amplitude of Refracted Waves for the Bottom Obstacle

where

$$P(x) = \begin{cases} P_0 & 0 \le x \le 0.3 \\ \frac{P_0}{2}\left[1 - \sin\left(\frac{\pi(x-0.5)}{0.4}\right)\right] & 0.3 \le x \le 0.7 \\ 0 & x \ge 0.7 \end{cases} \tag{34}$$

and where P_0 is the maximum pressure.

Initial conditions which could be specified on the free surface are

$$\frac{\partial \eta}{\partial t} = f_1(x) \qquad y = 0,\ t = 0 \tag{35}$$

and

$$\eta = f_2(x) \qquad y = 0,\ t = 0 \tag{36}$$

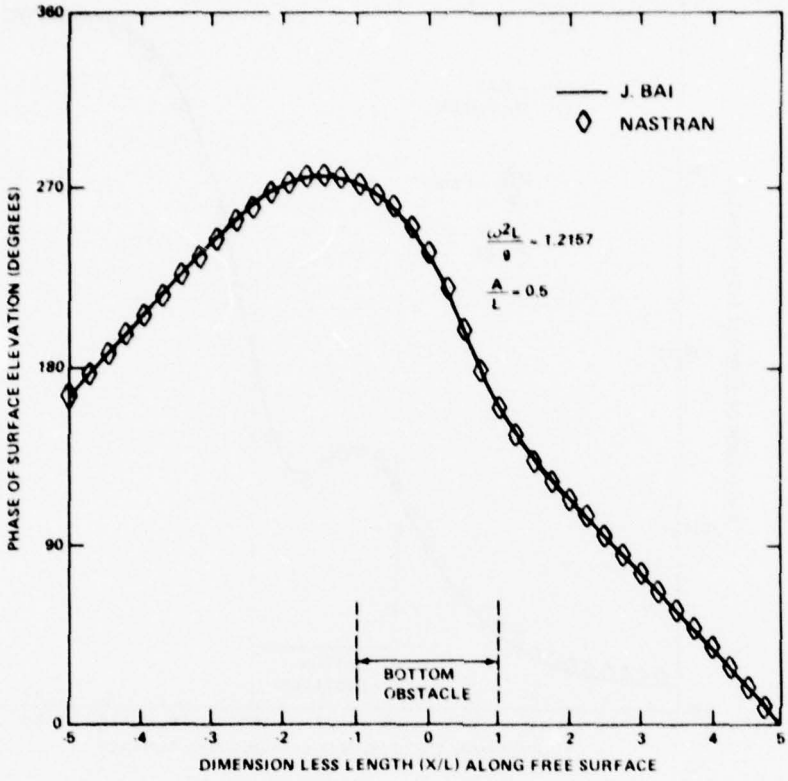

Figure 8. Phase of Refracted Waves for the Bottom Obstacle

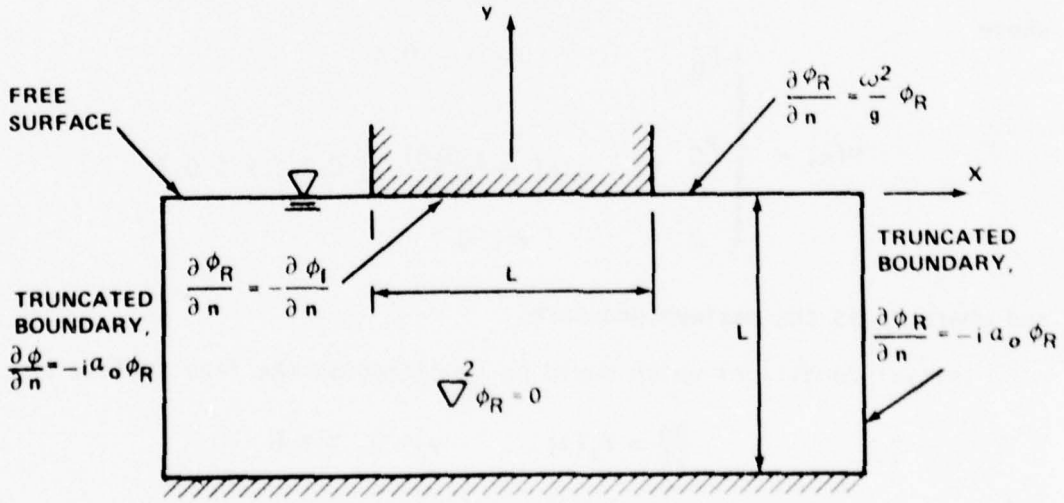

Figure 9. Geometry and Boundary Conditions for Refracted Waves Due to a Surface Obstacle

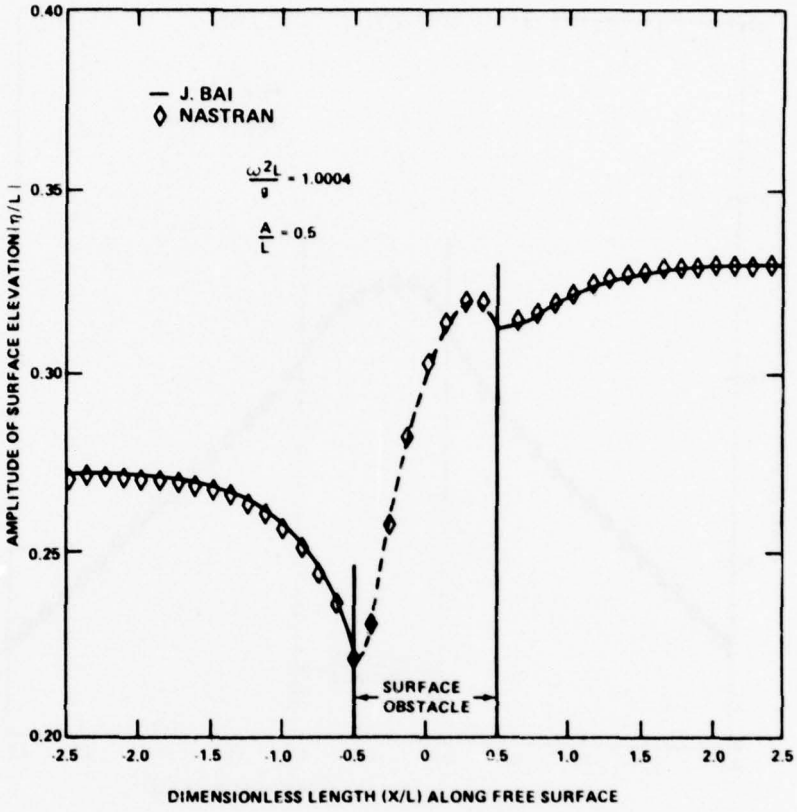

Figure 10. Amplitude of Refracted Waves for the Surface Obstacle

Eqs. (35) and (36) must be put in terms of Φ and $\partial\Phi/\partial t$ since this is the only suitable input to NASTRAN. Specifying $\partial\eta/\partial t$ on y=0 is equivalent by Eq. (3) to specifying $\partial\Phi/\partial y$ on y=0. Then Laplace's equation may be solved with the boundary conditions shown in Fig. 12, except that $\partial\Phi/\partial y$ is specified on the free surface. This will determine Φ everywhere initially. Similarly, specifying η on y=0 is equivalent by Eq. (4) to specifying $\partial\Phi/\partial t$ on y=0. Then the procedure just described may be repeated to determine $\partial\Phi/\partial t$ everywhere initially, since $\partial\Phi/\partial t$ also satisfies Laplace's equation and the boundary conditions shown in Fig. 12 (not including the free surface condition). This determines Φ and $\partial\Phi/\partial t$ everywhere initially.

The variational form for the free surface problem shown in Fig. 12, based on Hamilton's principle (see Courant and Hilbert, ref. 18), is

$$F(\Phi) = \frac{1}{2}\int_0^{t_1}\int_A \{(\frac{\partial\Phi}{\partial x})^2 + (\frac{\partial\Phi}{\partial y})^2\}dA\,dt + \int_0^{t_1}\int_B (\frac{1}{2}\gamma\Phi^2 + \beta\Phi)ds\,dt + \int_0^{t_1}\int_{\text{Free Surface}} \frac{1}{2g}(\frac{\partial\Phi}{\partial t})^2\,dx\,dt + \int_0^{t_1}\int_{\text{Free Surface}} \frac{1}{\rho g}\frac{\partial p}{\partial t}\Phi\,dx\,dt \qquad (37)$$

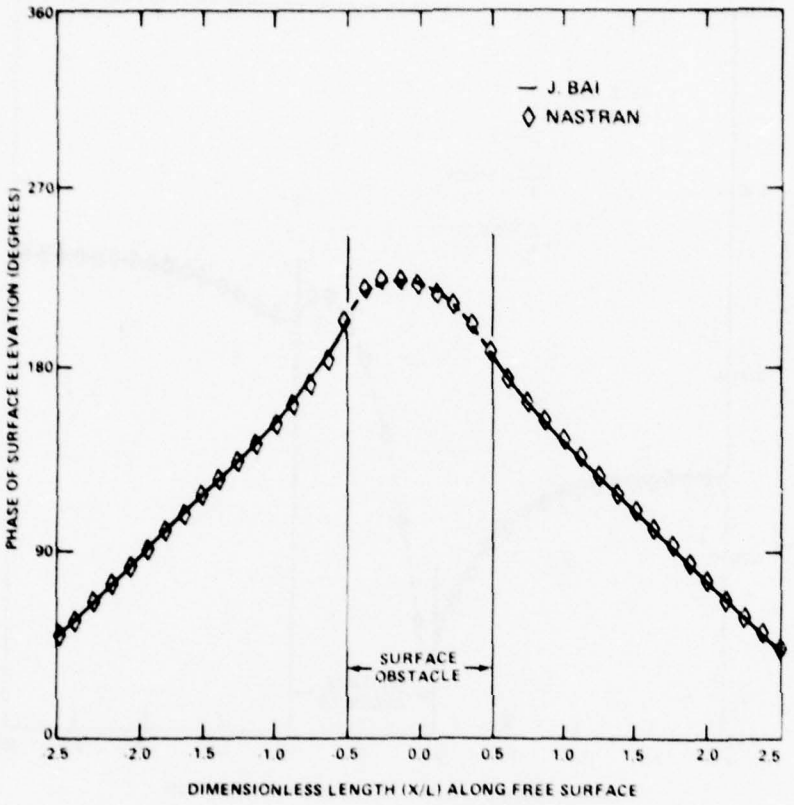

Figure 11. Phase of Refracted Waves for the Surface Obstacle

where B is the boundary of the region A, and all geometric boundary conditions are enforced. If variations of $F(\phi)$ taken with respect to ϕ equal zero, Eqs. (1), (5), (18), (35), and (36) are satisfied for zero initial conditions ($f_1=f_2=0$ in Eqs. (35) and (36)). Non-zero initial conditions can be easily incorporated into Eq. (37).

The finite element representation based on Eq. (37) was implemented using NASTRAN by modeling the fluid with QDMEM1 elements where material properties are given by Eq. (21). Any translational degree of freedom can be used to correspond to ϕ, but all remaining degrees of freedom are permanently constrained. The analysis method chosen is NASTRAN's Rigid Format 9, with the governing equation given by

$$\underline{M}\,\ddot{\underline{\phi}} + \underline{B}\,\dot{\underline{\phi}} + \underline{K}\,\underline{\phi} = \underline{F}(t) \qquad (38)$$

The stiffness matrix $\underline{K}$ generated by the QDMEM1 elements is equivalent to the finite element representation of the first term of Eq. (37).

The last two terms of Eq. (37) represent the free surface condition and may be incorporated into NASTRAN as follows: Let ϕ for any point on the free

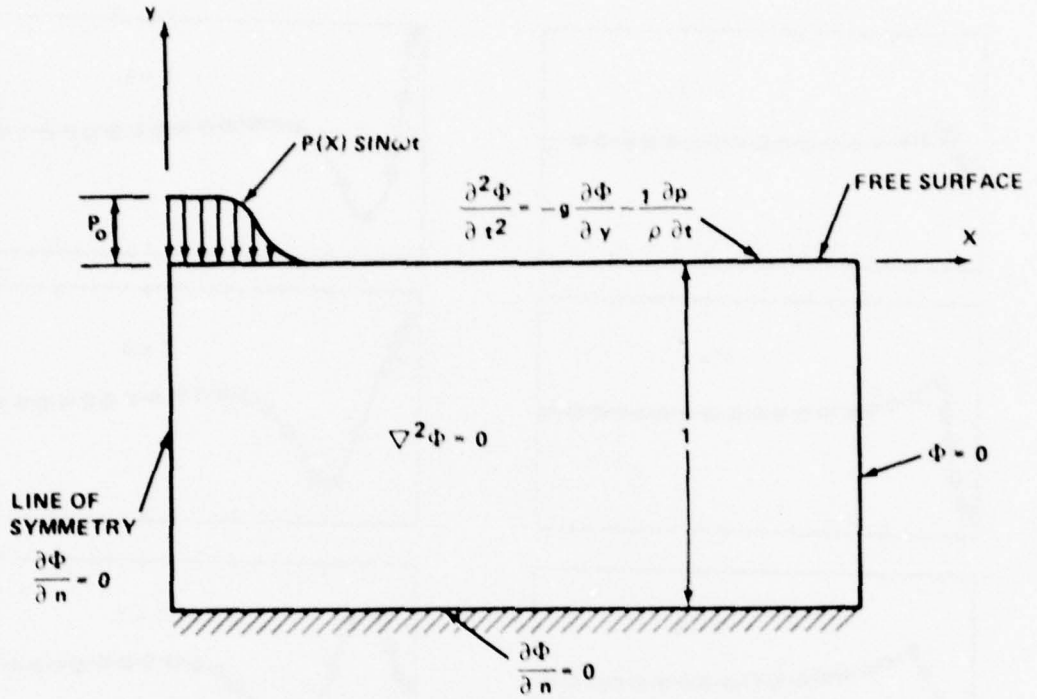

Figure 12. Stationary Pressure Distribution Oscillating on Free Surface

surface be given by

$$\Phi = \Sigma N_i \Phi_i \tag{39}$$

where N_i is the shape function for node i and Φ_i is the nodal potential. Then the finite element formulation for the third term of Eq. (37) is implemented using NASTRAN by inserting the matrix

$$(M2PP)_{ij} = \frac{1}{g}\int_{\substack{\text{Free}\\\text{Surface}}} N_i N_j \, dx \tag{40}$$

into the mass matrix $\underline{M}$ in Eq. (38). The finite element representation of the last term of Eq. (37) is impiemented using NASTRAN by inserting the vector

$$F_i = -\int_{\substack{\text{Free}\\\text{Surface}}} \frac{1}{\rho g}\frac{\partial p}{\partial t} N_i \, dx \tag{41}$$

into the forcing function $\underline{F}(t)$ in Eq. (38).

Referring to Fig. 12, the natural boundary condition $\partial\Phi/\partial n = 0$ (corresponding to $\gamma = \beta = 0$) on the bottom and left face is automatically

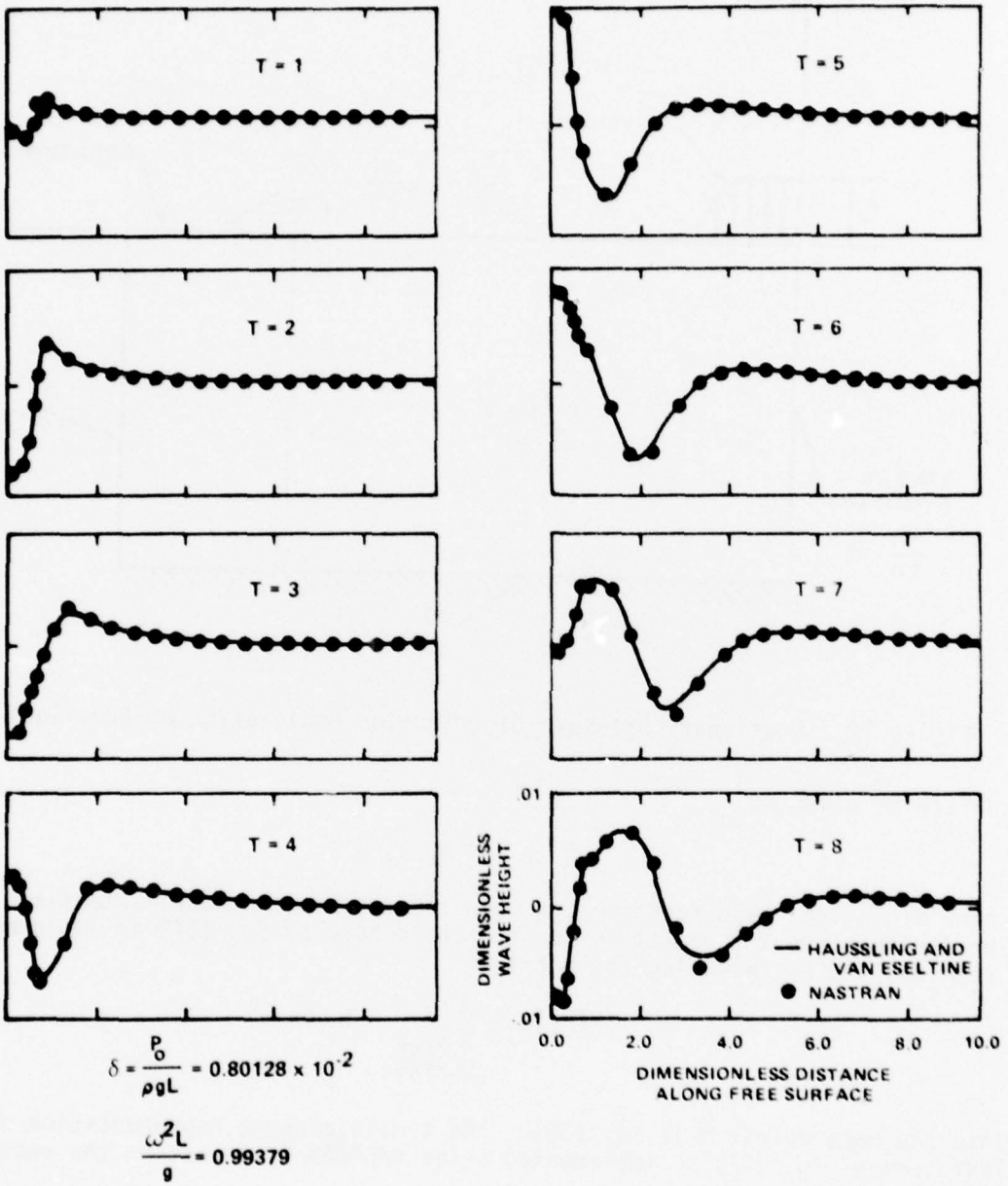

Figure 13. Development of Surface Elevations for the Pressure Distribution Problem

satisfied. The geometric boundary condition $\psi = 0$ is implemented by constraining $\psi_i = 0$ at all nodes i on the downstream boundary.

The above procedure was used to model the geometry and boundary conditions shown in Fig. 12. All variables have been put in dimensionless form using the pressure P_0, the depth L, and the gravitational constant g.

This procedure was used to model the geometry and boundary conditions shown in Fig. 12. QDMEM1 elements were used with dimensionless spacing $\Delta x = 0.1$ to 0.5, and $\Delta y = 0.25$; this would correspond to approximately 13 to 60 nodes per wave length, where the wave length is based on the steady state problem. A dimensionless time step of $\Delta t = .1$ was used. Rules of thumb for estimating spacing and time steps are given by Visser and van der Wilt (ref. 9). In this case approximately 60 time steps per period of the forcing function were used.

In Fig. 13, the NASTRAN results are compared to a Fourier series solution given by Haussling and Van Eseltine (ref. 19). The wave heights are in good agreement with the series solution and illustrate the capability of NASTRAN to model transient water wave problems.

STEADY STATE PROBLEMS

Consider the steady state problem shown in Fig. 14 where a cylinder of diameter L is moving at constant velocity U below the free surface. Steady state solutions are sought for which all variables are independent of time when referenced to a coordinate system moving with the body, that is, the x-y coordinate system shown in Fig. 14. In this coordinate system it can be shown that the potential ϕ must satisfy Laplace's equation, and the free surface condition expressed in Eq. (6) becomes (with p=0 on free surface)

$$\frac{\partial \phi}{\partial y} = - \frac{U^2}{g} \frac{\partial^2 \phi}{\partial x^2} \tag{42}$$

The boundary condition on the rigid cylinder shown in Fig. 14 is

$$\frac{\partial \phi}{\partial n} = - U \cos \theta \tag{43}$$

where θ is the angle between the x-direction and the normal to the body directed out of the fluid. No upstream waves are allowed and the Froude number,

$$F = \sqrt{\frac{U^2}{gL}}$$

is such that downstream waves are allowed (see Bai, ref. 6). Considerable effort was devoted to developing tractable radiation conditions for the upstream and downstream boundaries, resulting in the conclusion that none were possible. For this reason a series expansion is used in the regions beyond the upstream and downstream truncated boundaries and matched (at these boundaries) to the finite element solution. This technique was developed and successfully applied by Bai for both steady state problems (ref. 6) and frequency response problems (ref. 4). A similar finite element-series expansion technique for an acoustical fluid has been implemented using NASTRAN by Zarda (ref. 20).

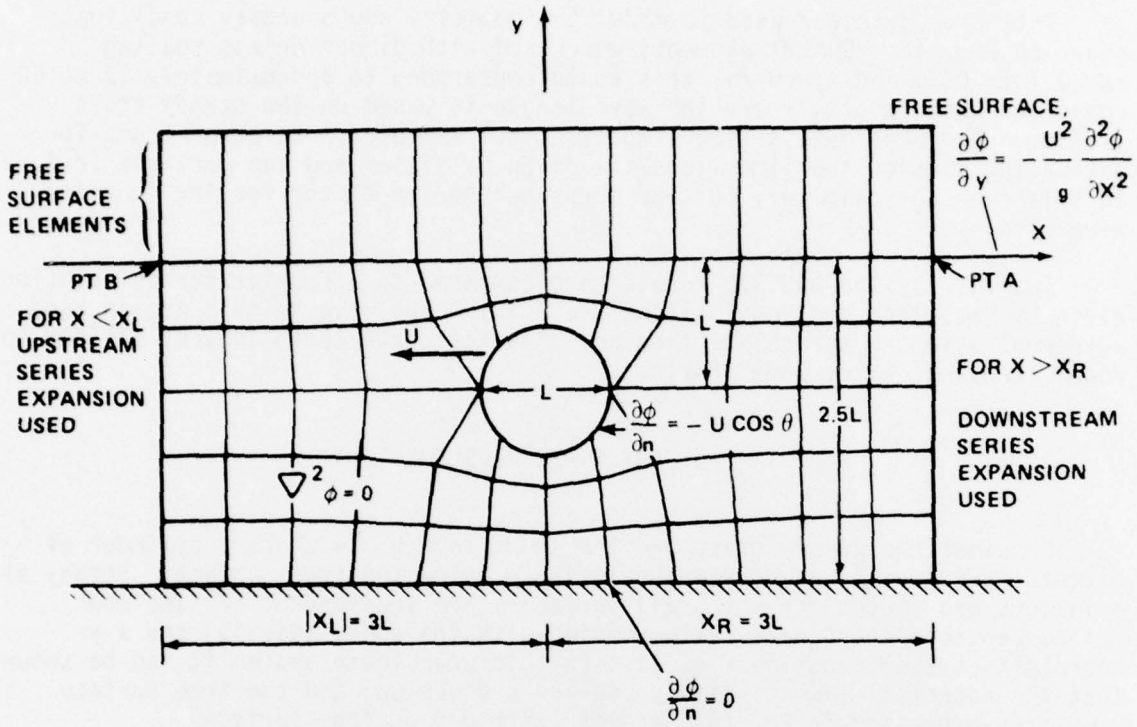

Figure 14. Finite Element Model for Cylinder Moving Below the Free Surface - Coarse Grid

It can be shown, using separation of variables, that downstream from the body

$$\phi = \sum_{j=1}^{N+3} A_j f_j \tag{44}$$

where

$$f_j = \begin{cases} \cos \alpha_j (y+d) e^{\pm \alpha_j x} & 1 \le j \le N \\ 1 & j = N+1 \\ \dfrac{\cosh \alpha_0 (y+d)}{\cosh \alpha_0 d} \cos \alpha_0 x & j = N+2 \\ \dfrac{\cosh \alpha_0 (y+d)}{\cosh \alpha_0 d} \sin \alpha_0 x & j = N+3 \end{cases} \tag{45}$$

and

$$\frac{U^2}{g}\alpha_0 = \tanh \alpha_0 d \ , \quad \frac{U^2}{g}\alpha_j = \tan \alpha_j d$$

Upstream from the body,

$$\phi = \sum_{j=1}^{N+1} B_j f_j \tag{46}$$

The sign in the exponential is (+) for the upstream boundary, and (-) for the downstream boundary. Furthermore, N is the number of series terms chosen (the same number is assumed upstream and downstream, although this is not necessary), and d is the depth. Eqs. (44) and (46) satisfy Laplace's equation and the boundary conditions on y=0 and y=-d. The first N terms represent local terms that decay away from the cylinder, and the last two terms in Eq. (44) represent an outgoing downstream wave; no such waves are allowed in the upstream expansion.

Consider the variational functional given by

$$F(\phi) = \frac{1}{2}\int_A \{(\frac{\partial\phi}{\partial x})^2 + (\frac{\partial\phi}{\partial y})^2\} dA - \frac{U^2}{2g}\int_{x_A}^{x_B} (\frac{\partial\phi}{\partial x})^2 dx + \int_{\text{Body}} U\cos\phi \, ds$$

$$\text{Free Surface} \tag{47}$$

$$- \int_{\substack{\text{Upstream} \\ x=x_L}} [\frac{\partial\phi}{\partial n}]_{x=-x_L} \phi \, dy - \int_{\substack{\text{Downstream} \\ x=x_R}} [\frac{\partial\phi}{\partial n}]_{x=x_R} \phi \, dy - \frac{U^2}{g}[\frac{\partial\phi}{\partial x}]_{\substack{x=x_R \\ y=0}} \phi_B + \frac{U^2}{g}[\frac{\partial\phi}{\partial x}]_{\substack{x=x_L \\ y=0}} \phi_A$$

where points A and B and boundaries x_L and x_R are defined in Fig. 14, and n is the normal to the boundary directed out of the fluid. If independent variations of F with respect to ϕ, ϕ_A, and ϕ_B are set equal to zero, then Laplace's equation and the boundary conditions shown in Fig. 14 are satisfied, and $\partial\phi/\partial n$ is continuous on the upstream and downstream boundaries. No variations of the bracketed expressions in Eq. (47) are allowed, and these expressions can be evaluated in terms of the series coefficients by taking the appropriate derivatives using Eqs. (44) and (46). This will increase the number of unknowns by the number (2N+4) of series coefficients. The corresponding additional equations come from requiring that the potential ϕ is continuous at the upstream and downstream boundaries. Let the finite element representation at the truncated boundaries be given by

$$\phi = \sum_{i=1}^{NN} N_i \phi_i \tag{48}$$

where NN is the number of nodes on the truncated boundary. Then, for continuity of ϕ on the downstream boundary, it is required that

$$\sum_{i=1}^{NN} N_i \phi_i = \sum_{k=1}^{N+3} A_k f_k \quad \text{on} \quad x=x_R \tag{49}$$

and on the upstream boundary

$$\sum_{i=1}^{NN} N_i \phi_i = \sum_{k=1}^{N+1} B_k f_k \quad \text{on} \quad x= x_L \tag{50}$$

Eq. (49) is multiplied by f_j, j=1 to N+2, and integrated from -d to 0. This gives a system of equations

$$\sum_{i=1}^{NN} G_{ij}\phi_i = \sum_{k=1}^{N+3} H_{jk} A_k \quad \text{on} \quad x=x_R, \; j= 1 \text{ to } N+2 \tag{51}$$

where

$$G_{ij} = \int_{-d}^{0} N_i f_j \, dy \qquad i = 1 \text{ to } NN, \; j = 1 \text{ to } N+3 \tag{52}$$

and

$$H_{jk} = \int_{-d}^{0} f_j f_k \, dy \qquad j,k = 1 \text{ to } N+3 \tag{53}$$

Eqs. (51) are N+2 equations involving the N+3 unknowns A_k. Multiplying Eq. (49) by f_{N+3} and integrating from -d to 0 does not determine an independent equation since f_{N+2} is proportional to f_{N+3} for fixed x.

Multiplying Eq. (50) by f_j, j=1 to N+2, and integrating from -d to 0 gives

$$\sum_{i=1}^{NN} G_{ij}\phi_i = \sum_{k=1}^{N+1} H_{jk}B_k \qquad x = x_L, \; j = 1 \text{ to } N+2 \tag{54}$$

Eqs. (54) are N+2 equations in the N+1 unknowns B_k. The additional equation, determined by multiplying Eq. (50) by f_{N+2}, corresponds to the condition that no upstream waves are allowed (see Bai, ref. 6). Eqs. (51) and (54) give the additional 2N+4 equations involving the 2N+4 unknowns A_j and B_j.

The procedure just described can be modeled using NASTRAN. CIS2D8 elements are used to model the fluid (see refs. 21 and 22). These second order isoparametric elements with the material properties given by Eq. (21) determine a stiffness matrix equivalent to the finite element representation of the first term of Eq. (47).

The second term of Eq. (47) is modeled using additional CIS2D8 elements along the free surface as shown in Fig. 14. For these elements, the height in the y-direction is unity, and all nodes having the same value of x are constrained to move together. This is equivalent to having 1-D isoparametric

elements along the free surface. The material properties for these elements are given by Eq. (21) except that the material matrix $\underline{G}$ is multiplied by the constant factor $(-U^2/g)$.

The third term of Eq. (47) represents a loading term. It is implemented using NASTRAN by entering

$$F_i = - \int_{\text{Body}} U \cos \theta \, N_i \, ds \tag{55}$$

as nodal forces, where N_i is the shape function for node i on the body.

The fourth and fifth terms of Eq. (47) represent coupling terms at the upstream and downstream boundaries. Using Eqs. (44) and (46) to determine the normal derivatives, the finite element modeling yields, for the downstream boundary,

$$(K2PP)_{i,j} = \sum_{j=1}^{N+3} \int_{-d}^{0} - \frac{\partial f_j}{\partial x} \bigg|_{x=x_R} N_i \, dy \qquad \begin{matrix} i = 1 \text{ to } NN \\ j = 1 \text{ to } N+3 \end{matrix} \tag{56}$$

where the matrix K2PP is added to the stiffness matrix. In order to implement this condition, N+3 scalar unknowns A_j are created using SPOINT data cards. Then the matrix term $(K2PP)_{i,j}$ in Eq. (56) refers to node i on the downstream boundary and to the SPOINT representation of the unknown A_j. Similarly, for the upstream boundary

$$(K2PP)_{i,j} = \sum_{j=1}^{N+1} \int_{-d}^{0} \frac{\partial f_j}{\partial x} \bigg|_{x=x_L} N_i \, dy \qquad \begin{matrix} i = 1 \text{ to } NN \\ j = 1 \text{ to } N+1 \end{matrix} \tag{57}$$

For the last two terms in Eq. (47), the finite element representation yields

$$(K2PP)_{B,j} = - \frac{U^2}{g} \frac{\partial f_j}{\partial x} \bigg|_{x=x_R} \qquad j = 1 \text{ to } N+3 \tag{58}$$

$$(K2PP)_{A,j} = \frac{U^2}{g} \frac{\partial f_j}{\partial x} \bigg|_{x=x_L} \qquad j = 1 \text{ to } N+1 \tag{59}$$

Eqs. (51), (54), and (56) through (59) are entered into NASTRAN using DMIG cards and complete the set of equations to solve for the nodal potentials and the upstream and downstream series coefficients. NASTRAN's Rigid Format 1 (Static Analysis) does not accept DMIG cards. Therefore, Rigid Format 9 was used for one time step. (Since no mass or damping matrix exists, static equilibrium is reached for any time step.)

Computations, with all quantities being non-dimensionalized with respect to the cylinder diameter L, velocity U, and fluid density ρ, were carried out using NASTRAN for the grids shown in Figs. 14 and 15. Each mesh has approximately the same number of unknowns since the series solution is used for $|x| \geq 3.0$ on the coarse grid and for $|x| \geq 1.5$ on the fine grid. Approximately 9 and 17 nodes per wave length were used for the coarse and fine grids, respectively.

Wave height along the free surface is plotted in Fig. 16. Results for both the coarse and fine NASTRAN grids are seen to compare favorably with a solution obtained by Giesing and Smith (ref. 23) using a distribution of sources. The solutions shown here all satisfy the condition that no upstream waves are allowed. (In this case, since the Froude number based on the depth is less than one, downstream waves are generated.)

The pressure distribution on the cylinder may be determined from Bernoulli's equation. Assuming the flow about the cylinder is steady, then, in the x-y coordinate system that is moving with the body, Eq. (2) becomes

$$p = -\rho U \frac{\partial \phi}{\partial x} - \frac{1}{2}\rho\left\{\left(\frac{\partial \phi}{\partial x}\right)^2 + \left(\frac{\partial \phi}{\partial y}\right)^2\right\} \tag{60}$$

Fig. 17 illustrates a plot of the dimensionless pressure as a function of the x coordinate on the surface of the cylinder. Results are shown for both the fine and coarse grids shown in Figs. 15 and 16. The discontinuities of the curves occur at element junctures on the cylinder. Although the potential ϕ is necessarily continuous, $\partial\phi/\partial x$ and $\partial\phi/\partial y$ are not necessarily continuous within the finite element approximation, and discontinuities in these terms are magnified in determining the pressure in Eq. (60). Also shown in Fig. 17 is a table showing computed values of the wave resistance and lift coefficients, C_D and C_L, defined by

$$(\rho U^2 L)C_D = -\int_{\text{Body}} p\, dy \tag{61}$$

$$(\rho U^2 L)C_L = \int_{\text{Body}} p\, dx \tag{62}$$

The values of C_D and C_L computed using NASTRAN compare favorably with those given by Giesing and Smith (ref. 20).

CONCLUSIONS

The problems illustrated here demonstrate the capability of NASTRAN to successfully model linearized free surface flow problems for harmonic, transient, and steady state cases. Although the results presented here are for arbitrary 2-D and axisymmetric geometries, the procedures described are directly applicable to 3-D flow problems and readily extendable to the coupled problem of fluid flow about an elastic body.

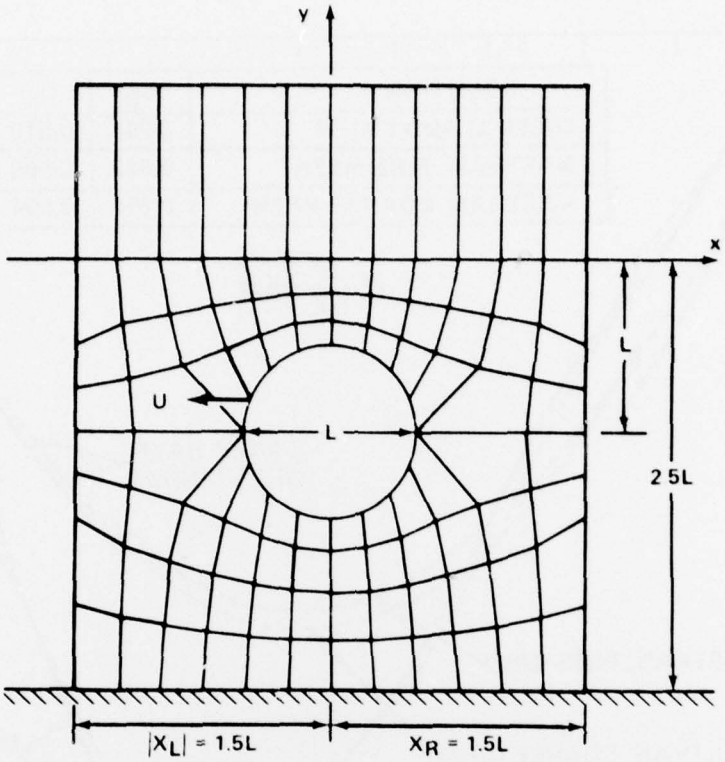

Figure 15. Finite Element Model for Cylinder Moving Below the Free Surface - Fine Grid

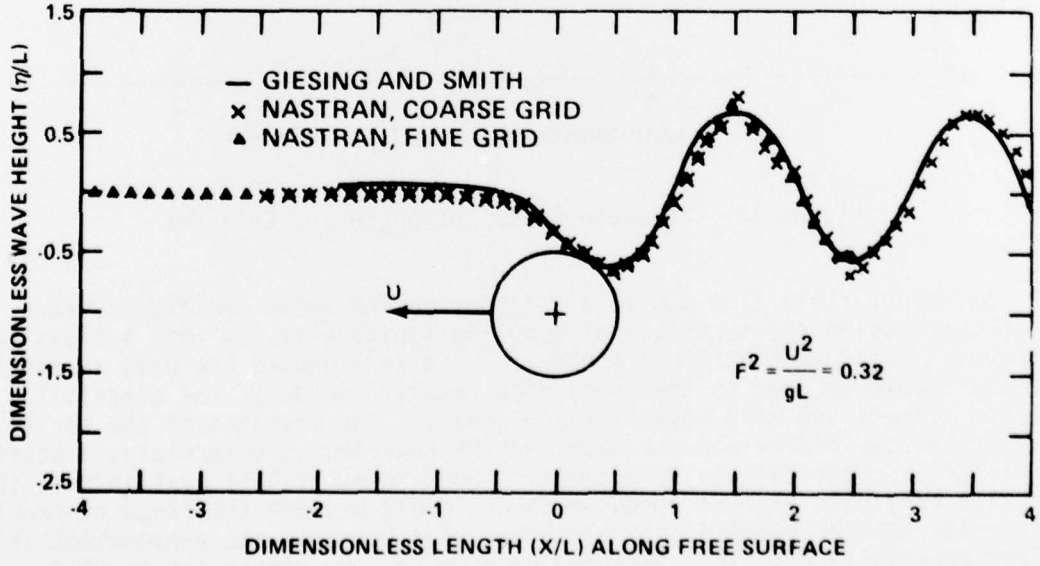

Figure 16. Wave Height Along the Free Surface for Moving Cylinder

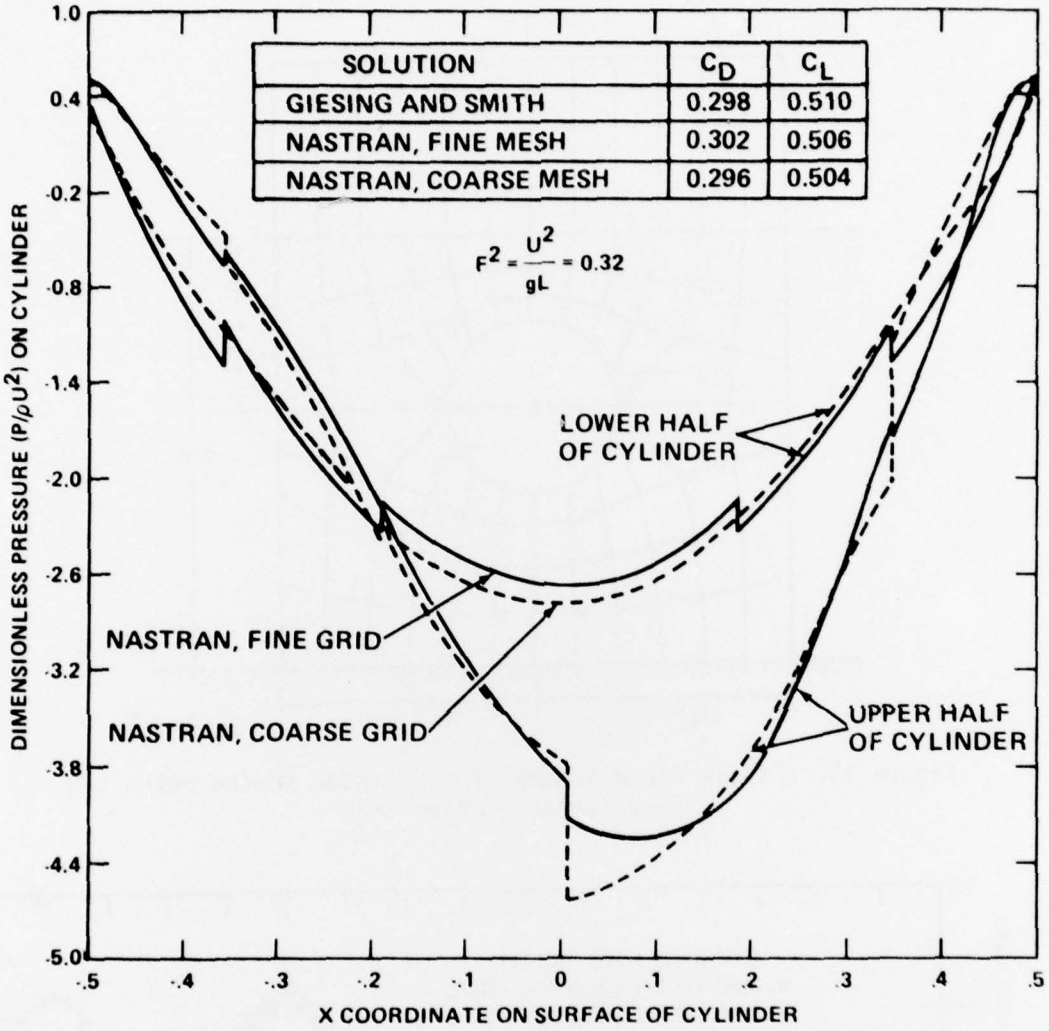

Figure 17. Pressure Distribution on the Cylinder

The steady-state flow due to a cylinder moving below the free surface was computed using the technique of coupling finite elements with a classical method at an appropriate common boundary. Finite elements are used to model irregular geometry over to some specified regular boundary, and classical solution methods are used beyond this boundary. The coupling of the series solutions to the finite element model may be regarded as determining a stiffness matrix for a "classical finite element." Such "elements", if available in the libraries of finite element computer codes, would broaden the range of problems efficiently handled using finite elements. Furthermore, the enhancement of the NASTRAN capability described here may be used to investigate the coupled

problem of fluid flow about an elastic body near or on a free surface. In such a case both the structure and surrounding fluid would be modeled using existing NASTRAN elements and would be coupled at the fluid-structure interface.

REFERENCES

1. Wehausen, J.V., The Motion of Floating Bodies. Annual Review of Fluid Mechanics, vol. 3, 1971, pp. 237-268.

2. Hess, J.L. and Smith, A.M.O., Calculation of Potential Flow About Arbitrary Bodies. Progress in Aeronautical Sciences, vol. 8, 1967, pp. 1-137.

3. Bai, K.J., A Variational Method in Potential Flows With a Free Surface. College of Engineering, Univ. of Calif., Report No. NA 72-2, 1972.

4. Bai, K.J. and Yeung, R.W., Numerical Solutions to Free-Surface Flow Problems. Tenth Symposium on Naval Hydrodynamics, 1974. Cooper, R.D. and Doroff, S.W., editors.

5. Bai, K.J., Diffraction of Oblique Waves by an Infinite Cylinder. J. Fluid Mechanics, vol. 68, part 3, 1975, pp. 513-535.

6. Bai, K.J., A Localized Finite-Element Method for Steady, Two-Dimensional Free-Surface Flow Problems. Proceedings of the First International Conference on Numerical Ship Hydrodynamics. Schot, J.W. and Salvesen, N., editors, October 1975, pp. 209-229.

7. Berkhoff, J.C.W., Computation of Combined Refraction-Diffraction. Proceedings 13th Coastal Engineering Conference, 2, ASCE, 1972, pp. 471-490.

8. Chen, H.S. and Mei, C.C., Oscillations and Wave Forces in a Man-Made Harbor in the Open Sea. The 10th Symposium on Naval Hydrodynamics, Office of Naval Research, 1974.

9. Visser, W. and van der Wilt, M., A Numerical Approach to the Study of Irregular Ship Motions. Finite Elements in Fluids, vol. 1, Gallagher et al., editors, 1975, pp. 233-249.

10. The NASTRAN Theoretical Manual. NASA SP-221(03), Washington, D.C., 1976.

11. The NASTRAN User's Manual. NASA SP-222(03), Washington, D.C., 1976.

12. Everstine, G.C. and McKee, J.M., A Survey of Pre- and Post-processors for NASTRAN. Structural Mechanics Computer Programs: Surveys, Assessments, and Availability, Pilkey et al., editors, Univ. Press of Virginia, Charlottesville, 1974, pp. 825-843. Also published as NSRDC Report 4391 (1974).

13. Stoker, J.J., Water Waves. Interscience Publishers, N.Y., 1957.

14. Everstine, G.C., Schroeder, E.A., and Marcus, M.S., The Dynamic Analysis of Submerged Structures. NASTRAN: User's Experiences, NASA TM X-3278, Sept. 1975, pp. 419-429.

15. Schroeder, E.A. and Marcus, M.S., Finite Element Solution of Fluid-Structure Interaction Problems. David Taylor Naval Ship Research and Development Center, Report 76-0145, Oct. 1976.

16. Marcus, Melvyn S., A Finite Element Method Applied to the Vibration of Submerged Plates. Journal of Ship Research, to appear.

17. Everstine, G.C., A NASTRAN Implementation of the Doubly Asymptotic Approximation for Underwater Shock Response. NASTRAN: Users' Experiences, NASA TM X-3428, Oct. 1976, pp. 207-228.

18. Courant, R. and Hilbert, D., Methods of Mathematical Physics. Interscience Publishers, New York, 1963, vol. I.

19. Haussling, H.J. and Van Eseltine, R.T., Unsteady Air-Cushion Vehicle Hydrodynamics Using Fourier Series. Journal of Ship Research, vol. 20, no. 2, June 1976, pp. 79-84.

20. Zarda, P.R., A Finite Element-Analytical Method for Modeling a Structure in an Infinite Fluid. NASTRAN: Users' Experiences, NASA TM X-3428, Oct. 1976, pp. 251-272.

21. Hurwitz, M.M., Additions to the NASTRAN User's Manual and Theoretical Manual for a Thermostructural Capability for NASTRAN Using Isoparametric Finite Elements. David W. Taylor Naval Ship Research and Development Center, Report 4134, 1973.

22. Hurwitz, M.M., Programmer's Manual Additions and Demonstration Problems for a Thermostructural Capability for NASTRAN Using Isoparametric Finite Elements. David W. Taylor Naval Ship Research and Development Center, Report 4656, 1975.

23. Giesing, J.P. and Smith, A.M.O., Potential Flow About Two-Dimensional Hydrofoils. J. Fluid Mechanics, vol. 28, Part I, 1967, pp. 113-129.

INITIAL DISTRIBUTION

Copies	
1	DNA/E. Sevin
1	USA RES OFF/CRD-AA-IPL
8	CHONR
	1 Code 102
	1 Code 430/R.J. Lundegard
	1 Code 430B/M. Cooper
	1 Code 432/L.D. Bram
	1 Code 434/T.C. Varley
	1 Code 436/B.J. MacDonald
	1 Code 438/R.D. Cooper
	1 Code 474/N. Perrone
1	NAVMAT/08T23
1	DNL
2	NRL
	1 H. Huang
	1 Lib
1	ONR/Boston
1	ONR/Chicago
1	ONR/London
1	ONR/Pasadena
1	USNA/Lib
2	NAVPGSCOL
	1 Library
	1 R. Newton
1	NAVWARCOL/Lib
1	ROTC, MIT/Lib
1	NOSC/Lib
1	NWC/Lib

Copies	
1	NSWC Dahlgren/Lib
2	NSWC White Oak
	1 S. Lucas
	1 Lib
2	NUSC NLONLAB
	1 A. Carlson
	1 Lib
1	NUSC NPT/Lib
5	NAVSEA
	1 SEA 03C
	1 SEA 0311
	1 SEA 033
	1 SEA 0351/C. Pohler
	1 SEA 09G32
1	NAVSHIPYD BREM/Lib
1	NAVSHIPYD CHASN/Lib
1	NAVSHIPYD MARE/Lib
1	NAVSHIPYD NORVA/Lib
1	NAVSHIPYD PEARL/Lib
1	NAVSHIPYD PHILA/Lib
1	NAVSHIPYD PTSMH/Lib
3	NAVSEC
	1 SEC 6150D/H. Ward
	1 SEC 6113B6/P.A. Gale
	1 SEC 6114/R.S. Johnson
12	DDC
1	BUSTAND/Lib
2	NASA HQS
	1 M. Chargin
	1 Lib

Copies	
3	NASA Ames Res Cen 1 E.D. Martin 1 R.W. MacCormack 1 Lib
1	NASA Goddard SFC/Lib
1	NASA Johnson Space Cen/Lib
1	NASA Kennedy Space Cen/Lib
1	NASA Langley Res Cen/Lib
1	NASA Lewis Res Cen/Lib
2	NASA Marshall SFC 1 R. McComas 1 Lib
2	NSF 1 Engr Sci Div 1 Math Sci Div

CENTER DISTRIBUTION

Copies	Code	Name
1	1100	W.M. Ellsworth
1	1500	W.E. Cummins
1	1504	V.J. Monacella
1	1520	R. Wermter
1	1521	P.C. Pien
1	1540	W.B. Morgan
4	1552	J.H. McCarthy K.J. Bai N.Salvesen C.H. VonKerczek
1	1561	C.M. Lee
1	1562	M. Martin
1	1564	J.P. Feldman
2	1572	M.D. Ochi D. Moran
1	1600	H.R. Chaplin
1	1606	T.C. Tai
1	1630	A.G. Ford
1	1700	W.W. Murray
1	1720	M.A. Krenzke
2	1720.3	R.F. Jones T.E. Reynolds
1	1730	A.B. Stavovy
1	1740	I.S. Hansen
1	1740.5	B. Whang
1	1770	E.W. Palmer
1	1800	G.H. Gleissner
1	1802.2	F.N. Frenkiel
1	1805	E.H. Cuthill
2	1809.3	D. Harris
1	1820	A.W. Camara
1	1840	H.J. Lugt
1	1843	J.W. Schot
15	1843	M. Marcus
1	1844	S.K. Dhir
15	1844	P.R. Zarda
1	1850	T. Corin
1	1870	
1	1890	G.R. Gray
1	1900	M.M. Sevik
1	1960	D. Feit
1	1962	A. Zaloumis
2	1965	M. Clark Y.N. Liu
1	27	
1	2731	S. Brown

Copies	Code	Name
1	2744	Y.P. Lu
1	28	R.J. Wolfe
10	5214.1	Reports Distribution
1	522.1	Unclassified Lib (C)
1	522.2	Unclassified Lib (A)

DTNSRDC ISSUES THREE TYPES OF REPORTS

1. DTNSRDC REPORTS, A FORMAL SERIES, CONTAIN INFORMATION OF PERMANENT TECHNICAL VALUE. THEY CARRY A CONSECUTIVE NUMERICAL IDENTIFICATION REGARDLESS OF THEIR CLASSIFICATION OR THE ORIGINATING DEPARTMENT.

2. DEPARTMENTAL REPORTS, A SEMIFORMAL SERIES, CONTAIN INFORMATION OF A PRELIMINARY, TEMPORARY, OR PROPRIETARY NATURE OR OF LIMITED INTEREST OR SIGNIFICANCE. THEY CARRY A DEPARTMENTAL ALPHANUMERICAL IDENTIFICATION.

3. TECHNICAL MEMORANDA, AN INFORMAL SERIES, CONTAIN TECHNICAL DOCUMENTATION OF LIMITED USE AND INTEREST. THEY ARE PRIMARILY WORKING PAPERS INTENDED FOR INTERNAL USE. THEY CARRY AN IDENTIFYING NUMBER WHICH INDICATES THEIR TYPE AND THE NUMERICAL CODE OF THE ORIGINATING DEPARTMENT. ANY DISTRIBUTION OUTSIDE DTNSRDC MUST BE APPROVED BY THE HEAD OF THE ORIGINATING DEPARTMENT ON A CASE-BY-CASE BASIS.